Effect of Ultrasonic Bonding Parameters on the Contact Resistance and Bondability Performances of CIGS Thin Film Photovoltaic Solar Panel

Hassan Basher, Muhammad Nubli Zulkifli, Azman Jalar, and Michael Daenen

***Abstract*—This article aims to investigate the optimal ultrasonic bonding parameter namely bonding pressure, bonding energy, and bonding amplitude that can minimize the contact resistance (R_c), maximize the peel strength, and identify the possible failure modes of ultrasonic Al bond on Mo back contact layer of copper indium gallium (de)selenide (CIGS) thin-film photovoltaic (TFPV) solar panel. The transmission line method was used to measure R_c and a peel test was carried out to measure the peel strength and the possible failure modes of ultrasonic Al bond on the Mo layer. Design of experiment using D-optimal method was utilized to evaluate the effect of the ultrasonic bonding parameter toward the R_c and peel strength of the Al bond on the Mo layer. Individual and combination of the ultrasonic bonding parameter have a significant effect on the quality of Al bonds on Mo back contact layer of CIGS TFPV solar panel. Possible failure modes could be identified through the application of the higher value of individual ultrasonic bonding parameter while keeping constant other bonding parameters and through the qualitative result of the load-displacement profile obtained from the peel test. However, sample 2 with bonding pressure of 3 bar, bonding energy of 20 Ws, and bonding amplitude of 7.7 μm is the best-optimized bonding parameter window that can be applied to obtain ultrasonic Al bond with lower R_c and higher peel strength. It was noted that bonding pressure is the most sensitive bonding parameter followed by bonding amplitude and bonding energy.**

***Index Terms*—Copper indium gallium (de)selenide (CIGS) solar panel, contact resistance, peel strength, ultrasonic Al bond, ultrasonic bonding failure modes.**

I. Introduction

ONE key factor of reducing the costs of photovoltaic (PV) systems is to increase efficiency, reliability, and the service lifetime of PV modules. To increase the reliability and the service lifetime of PV modules, one must understand the challenges involved. Manufacturing of thin-film photovoltaic (TFPV) modules requires a significant amount of challenges to meet desired energy and efficiency [1], [2]. Interconnection within and between TFPV modules is one of the crucial steps that will affect the efficiency and reliability of TFPV solar panels [3], [4]. There are several methods that have been used as interconnection in the fabrication of TFPV solar panel namely soldering, spot welding, laser welding, and conductive adhesive tape to name a few. But most of the methods used as interconnection in the fabrication of TFPV solar panels are lacking in providing higher efficiency and reliability. This is due to higher temperature created from the application of soldering, spot welding, and laser welding [5]–[7]. Besides, the usage of conductive adhesive tape cannot provide higher efficiency performance on TFPV solar panels due to higher contact resistance, while laser welding is known to be costly [8], [9].

Ultrasonic bonding is one of the methods that can be used to overcome the issues arising from using conventional interconnection or bonding methods due to inherent advantages derived from its solid-state process characteristics [10]. Ultrasonic bonding of dissimilar metals is created by applying different settings of bonding parameters namely, bonding force or pressure, bonding energy, bonding time, and bonding amplitude to name a few [11], [12]. Most of the studies that have been conducted focus on optimizing the ultrasonic bonding parameter windows, determining the bonding mechanisms, identifying the failure modes, and evaluating the reliability performance [13]–[15]. However, most of these studies are related to semiconductor production. While in the TFPV solar panel production, there is a lack of comprehensive studies that were conducted especially the bondability and reliability performances of ultrasonic Al bonds on Molybdenum, Mo back contact layer of copper indium gallium (de)selenide (CIGS) TFPV solar panel. The previous study by Xu *et al*. [5] has provided a preliminary study regarding the bonding quality and reliability of ultrasonic Al bond on Mo back contact layer of CIGS TFPV solar panel. However, there is still some room that could be filled especially in terms of bonding mechanisms and possible failure modes that could be created due to the inappropriate setting of the ultrasonic bonding parameter on the CIGS TFPV solar panel.

Every parameter of ultrasonic bonding has been identified to play a role to optimize the bonding strength and contact resistivity of the interconnection of CIGS TFPV solar panel [5],

Manuscript received November 21, 2020; accepted December 22, 2020. Date of publication January 13, 2021; date of current version February 19, 2021. This work was supported in part by the Ministry of Higher Education of Malaysia under the Fundamental Research Grant FRGS/1/2020/TKO/UNIKL/02/10 and in part by the Universiti Kuala Lumpur under Short Term Research under Grant str19087. *(Corresponding author: Muhammad Nubli Zulkifli.)*

Hassan Basher and Muhammad Nubli Zulkifli are with the Electrical Engineering Section, Universiti Kuala Lumpur, British Malaysian Institute, Gombak 53100, Malaysia (e-mail: yasr_yasr2001@yahoo.com; mnubliz@unikl.edu.my).

Azman Jalar is with the Institute of Microengineering and Nanoelectronic, Universiti Kebangsaan Malaysia, Selangor 43600 UKM, Malaysia (e-mail: azmn@ukm.edu.my).

Michael Daenen is with the Faculty of Engineering Technology, Hasselt University, 3590 Diepenbeek, Belgium (e-mail: michael.daenen@uhasselt.be).

Color versions of one or more of the figures in this article are available online at https://doi.org/10.1109/JPHOTOV.2020.3047295.

Digital Object Identifier 10.1109/JPHOTOV.2020.3047295

[16]. The methods used to evaluate the strength and resistivity of the ultrasonic bonding varies based on the applications. For example, TFPV solar panel interconnection usually used peel test and transmission line method (TLM) to evaluate the peel strength and contact resistance of the bonds, respectively. The peel test provides qualitative and quantitative results that are useful to obtain the bonding mechanisms and the peel strength [17], [18], whereas the TLM provides the contact resistance value of the bonds, which inversely related to the efficiency of TFPV solar panel [19]. However, most of the studies were focusing on the individual effect, which is either the electrical performance or the mechanical performance of ultrasonic bonding on the TFPV solar panel. Thus, a comprehensive comparison between peel test and TLM results could provide useful data to produce high-quality ultrasonic Al bonds on Mo back contact layer of CIGS TFPV solar panel in terms of mechanical and electrical performances.

Although ultrasonic metal welding is well qualified as an interconnection methodology, there is a lack of scientific quality guidelines for implementing ultrasonic bonding between Al ribbon and Mo back contact layer of CIGS TFPV solar panel. In the current study, the effect of the ultrasonic bonding parameter namely bonding pressure, bonding energy, and bonding amplitude toward the contact resistance and peel strength were evaluated using the TLM and peel tests, respectively. The effect of the ultrasonic bonding parameter toward the contact resistance and the peel strength of Al ribbon bonds was evaluated by conducting a design of experiment (DOE) using D-optimal method. The possible failure modes were identified through the application of the higher value of bonding parameter and peel test qualitative results of load-distance profiles. The relationship between contact resistance and peel strength was evaluated to obtain the most optimized bonding parameter for ultrasonic Al bonds on Mo back contact layer of CIGS TFPV solar panel.

II. Materials and Methods

Aluminum (Al) ribbon with thickness and width of 0.15 and 2 mm, respectively, was bonded onto the thin film Molybdenum (Mo) which is the back-metal contact for the CIGS thin-film solar panel using Schunk DS-35 ultrasonic bonder as shown in Fig. 1. Mo thin film or layer with a thickness of 0.26 μm is located on top of the glass substrate with a thickness of 3 mm was cleaned with isopropanol before the ultrasonic bonding process was carried out to get a good connection. The sonotrode (welder's head) used in the ultrasonic bonder has dimensions of 5 $\times$ 3 mm². Ultrasonic Al bonds were created based on the repeated process of departure, arrival, and touchdown (with application of ultrasonic bonding parameters) of sonotrode onto the Mo thin film. Fig. 2 illustrates the cross-sectional schematic view of ultrasonic Al bond, ribbon, and the direction of applied bonding pressure and amplitude. From Fig. 2, the repeated process of departure, arrival, and touchdown is starting from right to the left where the Al ribbon is departed to from first Al bond and arrived to the second Al bond location. Then the bonding pressure, ultrasonic maximum energy, and ultrasonic amplitude are applied to create the second Al bond on Mo layer of glass substrate. This process is repeated for the creation of the subsequent Al bond.

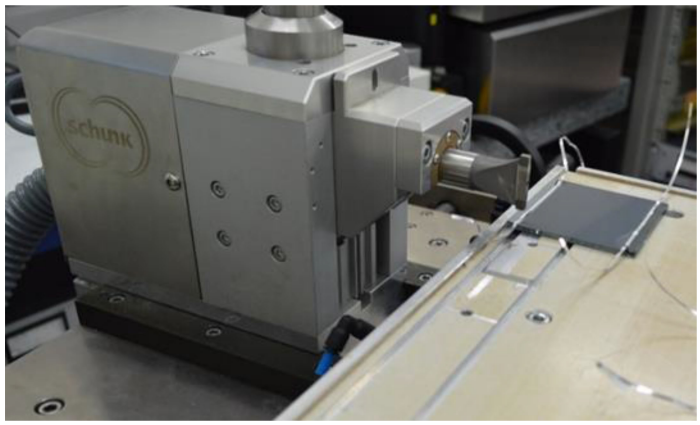

Fig. 1 Schunk DS-35 ultrasonic bonder.

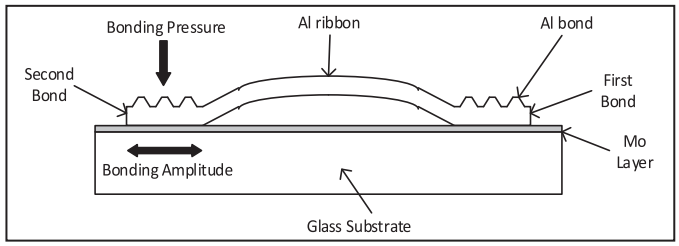

Fig. 2. Cross-sectional schematic view of ultrasonic Al bond and ribbon. Black arrows indicate the direction of bonding pressure and amplitude.

TABLE I
Ultrasonic Bonding Parameters

Parameter	Range
Pressure	1, 2, 2.5, 3, 3.5 (bar)
Maximum Energy	15, 17, 20, 23 (Ws)
Amplitude	7.7, 8.4, 9.1, 9.8 (μm)

Three ultrasonic bonding parameters namely pressure with a unit of bar, amplitude with a unit of μm, and maximum energy with a unit of Watt second or Ws have been chosen for the current study. These bonding parameters are the main parameters that have a major effect on the bondability of the ultrasonic bonding and has been widely reported by several research [5], [20]. Table I shows the ultrasonic bonding parameters with the range and unit used for the current study. Also, the preliminary test was conducted to identify the suitable parameter range and the possible failure modes by applying the higher or lower values of one of the ultrasonic bonding parameters, while others are kept constant at a certain value. According to Jordan *et al*. [21], failure mode is the cause of failure for the detachment of ultrasonic Al bonds. Pan *et al*. [22] have listed the possible failure modes for ultrasonic bonds such as heel break, foot lift, nonstick on pad, and ribbon break to name a few. Table II shows the experimental strategy for the preliminary test.

The effect of the ultrasonic bonding parameter toward the contact resistivity and the peel strength of Al bonds was evaluated by conducting the DOE in JMP software based on a custom design

TABLE II
EXPERIMENTAL STRATEGY FOR THE PRELIMINARY TEST

Sample	Pressure (bar)	Maximum Energy (Ws)	Amplitude (μm)
A	2	17	11.2
B	4	17	8.4
C	2	25	8.4

TABLE III
DOE FOR ULTRASONIC BONDING

Sample	Pressure (bar)	Maximum Energy (Ws)	Amplitude (μm)
1	2.5	23	8.4
2	3	20	7.7
3	1	15	8.4
4	1.5	15	7.7
5	3.5	17	8.4
6	1	17	7.7
7	3.5	20	7.7
8	1	20	8.4
9	1	20	9.1
10	1	23	7.7
11	3	15	8.4
12	2	20	8.4
13	3	23	9.1

using D-optimal method. D-optimal method was selected for the current study due to smaller number of experimental runs and also providing a comparable data to that of full factorial method [23]. Thirteen experimental runs of ultrasonic bonding were carried out based on the arrangement of the bonding parameters as shown in Table III. This has created 13 samples of Al bond with Mo layer.

On each sample, five until ten Al bonds and five Al ribbon lines of busbar were created as shown in Fig. 3. The TLM was used to measure the contact resistance, R_c between the Al bond and the Mo layer. The four-point method of TLM measurements was used to measure the contact resistance as shown in Fig. 3 [19], [24]. Current (I) and the voltage (V) of the sample were measured at room temperature under dark condition using four points probe method, where the current measured by a precise current meter of SourceMeter 2400 through four successive contacts by keeping a fixed voltage across those contacts. The TLM test structure consists of several electrodes with different of distances (L_s) between any two series electrodes as shown in Fig. 3(a) with distances of $L_1 = 3$ mm, $L_2 = 6$ mm, $L_3 = 10$ mm, and $L_4 = 15$ mm. The measurements of contact resistances are made between adjacent electrical contacts while the separation between the electrodes, L is varied [5], [25].

MTS Insight Electromechanical Testing Systems was utilized to conduct the peel test on the ultrasonic Al bond. The goal of a peel test is to determine the welding strength of the ultrasonic bonding between the Al bond and the Mo layer. The peel test was carried out to identify the optimal ultrasonic parameters that give good pull strength in a 90° peel test. The applied load rate of 5 mm/min of peel test was applied for the current study to make sure the application of peel load is in medium speed and not too fast that might influence the results.

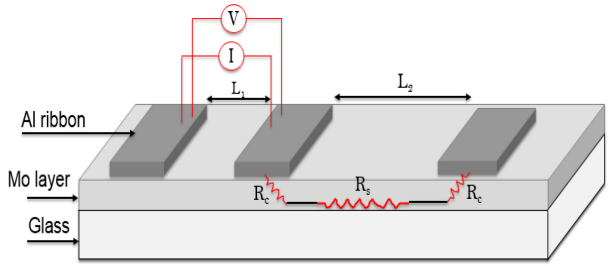

(a)

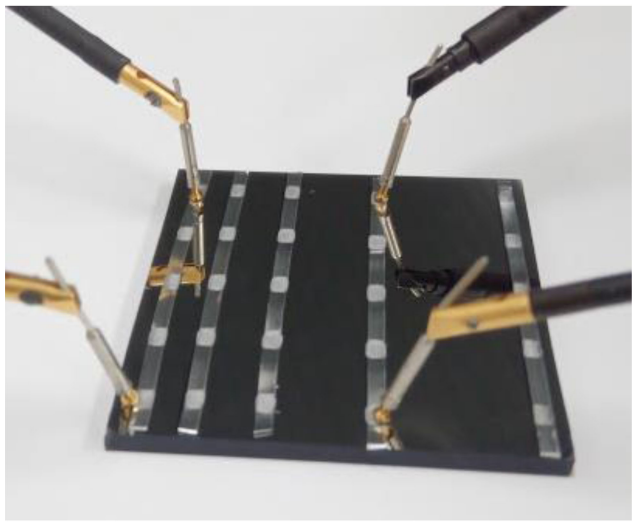

(b)

Fig. 3. TLM measurement. (a) Schematic. (b) Experimental setup.

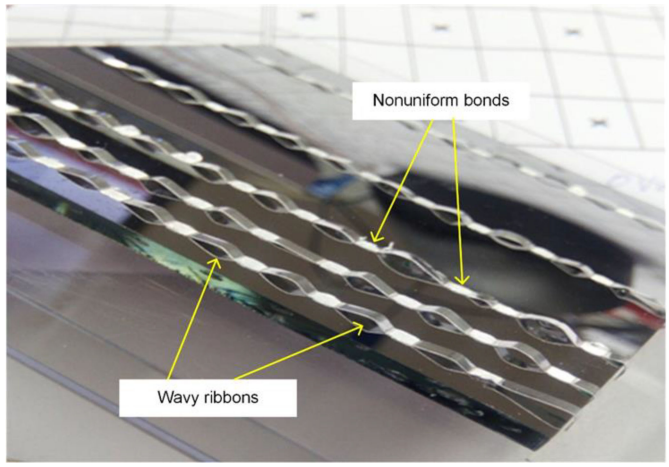

Fig. 4. Ultrasonic Al bonds from sample A with application of 11.2 μm of bonding amplitude.

III. RESULTS AND DISCUSSION

A. Preliminary Study

Figs. 4, 5, and 6 show the ultrasonic Al bonds based on the samples A, B, and C of Table II, respectively. In Fig. 4, it is shown that the application of higher bonding amplitude of more than 11.2 μm with other bonding parameters (pressure and maximum energy) are kept constant has made the ultrasonic Al

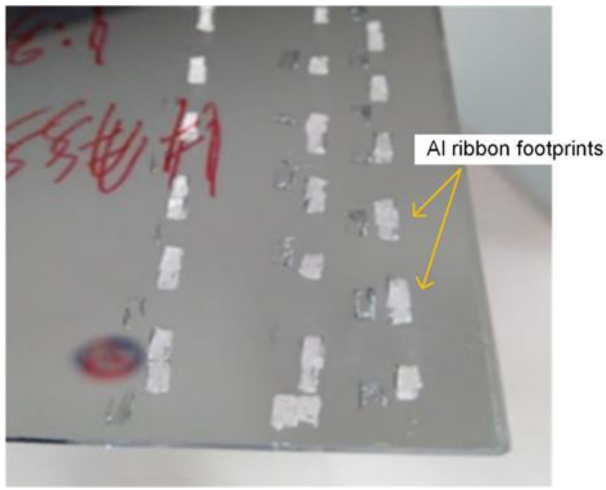

Fig. 5. Ultrasonic Al bonds from sample B with the application of 4 bar of pressure.

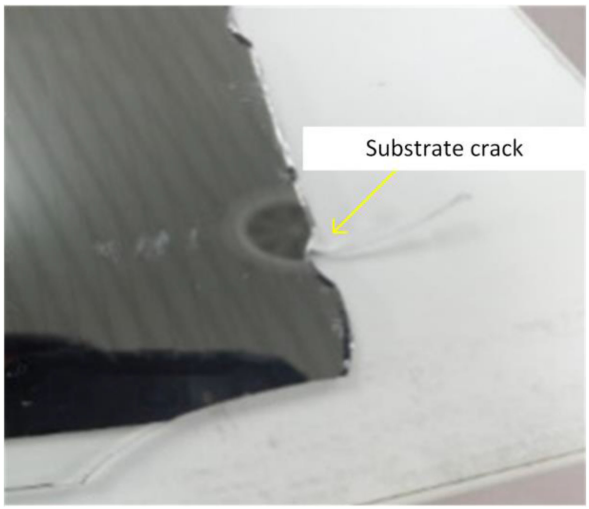

Fig. 6. Location of crack on the glass substrate from sample B with the application of 4 bar of pressure.

bonds in the nonuniform bonds, and Al ribbon located between each bond has a wavy shape rather than the straight shape. This is because the application of higher bonding amplitude could not provide enough elasticity for the ultrasonic Al bonds to have an appropriate departure and arrival of the touchdown of the sonotrode onto the Mo layer. This is because the higher application of amplitude can result in the strain hardening of the Al bond and ribbon due to the multiplication of dislocation [10], [26], [27]. A wavy shape Al ribbon and nonuniform bonds of ultrasonic Al ribbon bonds are also not preferable due to the gap created between the Al ribbon and Mo layer, which provides less contact area between Al ribbon and Mo layer. Subsequently, the conductivity between the Al ribbon and Mo layer is reduced where it also affects the reduction of the CIGS TFPV solar panel efficiency [5], [28]. In terms of the mechanical properties, the strain hardened and nonuniform Al bond has created less adhesion between the Al bond and Mo layer, which will lead to the reduction of bondability and the reliability performances of CIGS thin-film solar panel [4], [29], [30]. This is because

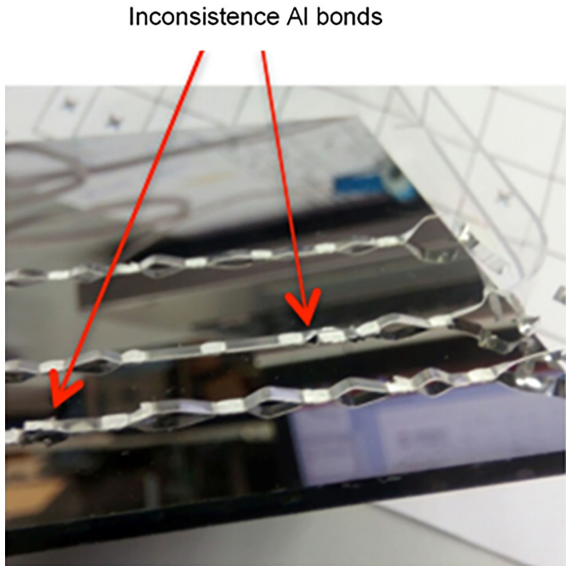

Fig. 7. Ultrasonic Al bonds from sample C with the application of 25 Ws of maximum energy.

the least adhesive ultrasonic Al bonds are more prone to initiate the crack at the bond interface that will lead to total detachment of the interconnection of the solar panel even at the early stage of operation [4], [5]. Thus, the application of higher bonding amplitude of 11.2 μm has created nonuniform ultrasonic Al bonds and a wavy shape of Al ribbon between each Al bond due to the excessive strain hardened and lack of elasticity of Al bond and ribbon.

Based on Fig. 5, it is noted that the application of higher bonding pressure of 4 bar with other parameters are kept constant, the ultrasonic Al bonds created on the Mo layer are not properly bonded and leave only the footprint of ultrasonic Al ribbon. This is because the application of higher bonding pressure or force has reduced the relative motion between the Al ribbon and Mo layer [31]. Relative motion between two dissimilar metals is important for the creation of microweld that created after the microslip and gross sliding phenomena [12], [32]. According to Takahashi *et al*. [33], the application of higher ultrasonic bonding pressure requires higher ultrasonic energy to compensate for the reduction of relative motion. For the current study, the ultrasonic bonding energy was kept constant, and this has led to the reduction of microweld creation or adhesion between the Al ribbon and Mo layer due to the higher application of bonding pressure. Besides, the application of higher bonding pressure also damages or breaks the glass substrate at multiple locations, especially near the edges as shown in Fig. 6. This could be due to the existence of edge chipping that is usually created during glass cutting process [34]. The edge chipping can act as the notch where the stress is concentrated and can initiate the crack propagation when experiencing excessive bonding pressure [35], [36]. Therefore, the application of higher bonding pressure of 4 bar has left only the footprint of the Al ribbon on the Mo layer and increase the potential of breaking the glass substrate, especially at the periphery or edge location.

In Fig. 7, it is noted that the ultrasonic Al bonds made on sample C with higher bonding energy of 25 Ws have inconsistent bonds, shape, and length of Al ribbon. Further analysis has been carried out to examine the surface of sonotrode after the ultrasonic bonding process of sample C of Table II, and it is noted there are some of the Al ribbon residues stuck on the sonotrode. The application of ultrasonic bonding energy has a direct effect on increasing the plastic deformation of metals due to the ultrasonic softening phenomenon [37], [38]. Furthermore, the required ultrasonic energy density to elongate or deform a metal is 10^7 times lower compared to that of heat [39], [40]. Also, the metal is work hardened or strengthened due to plastic deformation after being exposed to the ultrasonic energy excitation as compared to that of heat energy excitation. It is known that metal is annealed or softened due to the heat excitation power [26], [39]. The reason why it is important to compare between the application of ultrasonic bonding energy and heat is because both occur in different bonding technologies of ultrasonic bonding (current analysis) and ordinary welding or soldering, respectively. Therefore, the ultrasonic softening that happened during ultrasonic bonding and work hardening that happened after the ultrasonic bonding process are the contributing factors toward the inconsistency bond, shape, and length of the Al ribbon as shown in Fig. 7. Higher ultrasonic softening that happened during ultrasonic bonding process has deformed the Al ribbon quite excessively and can be identified through the broken Al ribbon bonds and Al ribbon residue stuck on the sonotrode as indicated in Fig. 7. Inconsistency in terms of bonds, shape, and length of Al ribbon is the subsequent effect that happened after the application of higher bonding energy where inconsistence volume of Al ribbon has stuck on the sonotrode or work-hardened Al bond could not provide consistent elongation for the departure and arrival of touchdown of sonotrode for the next ultrasonic Al bonding. Hence, the application of higher bonding energy of 25 Ws has created an ultrasonic Al bond with inconsistent bond, shape, and length of Al ribbon onto the Mo layer due to the combined effect of excessive ultrasonic softening and work hardening.

B. Contact Resistance

Fig. 8 illustrates the variation of contact resistance, R_c toward 13 samples of Al bonds based on the DOE of Table III. It is shown that each of the samples that have a different arrangement of ultrasonic bonding parameters has different R_c. It is desirable to have an Al ribbon bond with lower contact resistance to obtain a very high conductivity or efficiency of the CIGS TFPV solar panel [5], [28], [41]. The range of R_c values for the current study of 2.295 to 4.365 mΩcm^2 are significantly lower compared to that of soldering and adhesive tape interconnection technologies that have R_c values for about 100 and 1000 times, respectively [5]. However, it is in the interest of current study to identify the least R_c to be compared with the mechanical properties of peel strength of ultrasonic Al bonds. From Fig. 8, it is shown that Al bond from samples 12 and 13 is the most optimum ultrasonic bonding parameter windows with the lowest R_c of 2.295 mΩcm^2. R_c is known to have an inversely proportionate relationship with the contact area [42]. For the current analysis,

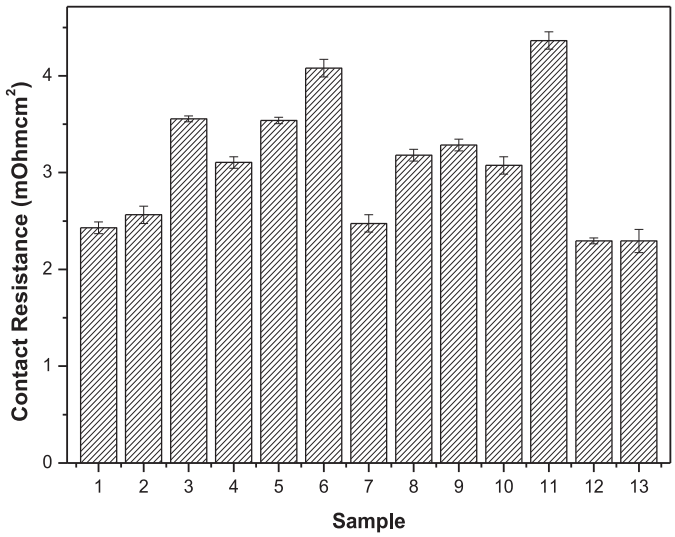

Fig. 8. Variation of contact resistance toward ultrasonic Al bonds.

two possible contact areas have been created between Al and Mo either directly and indirectly, namely, contact from Al bond and contact from Al ribbon, respectively. As mentioned earlier, each of the bonding parameters has a different effect on the bondability and shape of the Al ribbon either straight or wavy shapes. Thus, the cumulative contact area between the Al bonds and ribbon contribute toward decreasing the R_c that eventually increases the efficiency of CIGS TFPV solar panel with samples 12 and 13 having the lowest R_c of 2.295 mΩcm^2.

C. Load-Distance Profiles and Peel Strength

In addition to that of the R_c, 13 samples of Al bonds as indicated in Table III also have gone through the peel test to obtain the load-distance profile (qualitative result) and to measure the peel strength (quantitative result). Fig. 9 shows the graph or profile of load-distance of the peel test for samples 12, 10, and 4. From Fig. 9, it is noted that each load-distance graph has a different profile. For the current analysis, the direction of the peeling load is vertical to 90° direction or perpendicular to that of the direction of the distance of the Al bonds and ribbons. There are three types of load-distance profiles based on the number of segments that can be observed form the whole load-distance profiles of samples 1–13. One segment of load-distance profile is measured based on the number of the complete cycle of the lowest applied load of 0 N to the highest applied load and come back to the lowest applied load of 0 N. Fig. 9(a), (b), and (c) show the load-distance profile that has one segment from sample 12, two segments from sample 10, and three segments from sample 4, respectively. Table IV exhibits the list of Al bond samples with one, two, and three segments. From Fig. 9(b) and (c), it is shown that samples with two or three segments have a profile with multiple jumps of the load before decreasing to the lowest load. For the load-distance profiles with one segment as shown in Fig. 9(a), the transition is quite smooth before reaching the peak load and abruptly decreases with one or more steps to the lowest load of 0 N. The changes of distance with the increase of the constant rate of

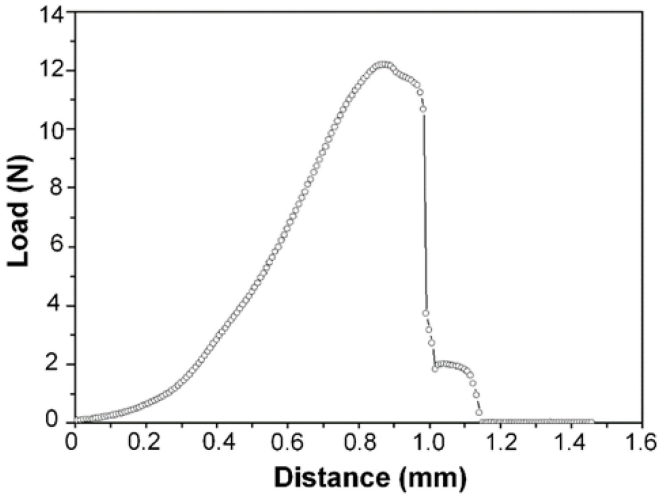

(a)

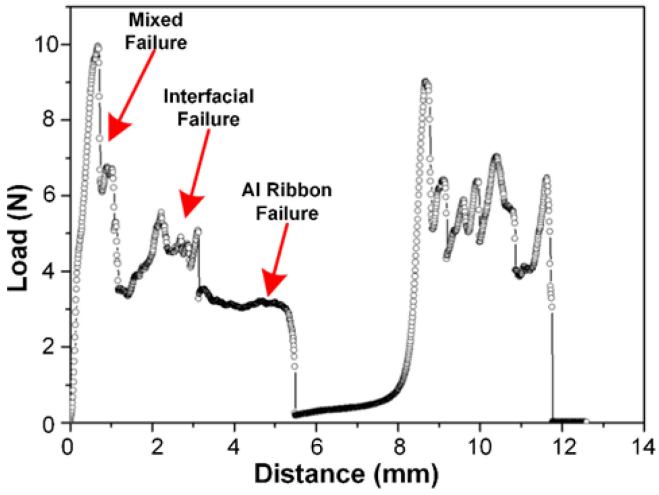

(b)

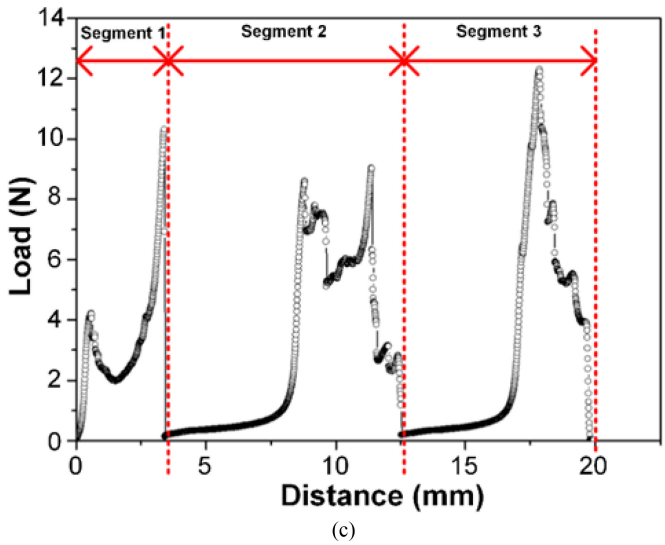

(c)

Fig. 9. Load-distance profiles of peel test for ultrasonic Al bonds from samples. a) 12 (one segment). b) 10 (two segments). c) 4 (three segments).

TABLE IV
LIST OF AL BOND SAMPLE WITH SEGMENTS OF PEAK AND TYPE OF FAILURE

Segment	Type of Failure Mode	Sample
1	Al ribbon failure	2, 3, 8, 9, 12, 13
2	Al ribbon failure, interfacial failure, mixed failure	1, 6, 7, 10, 11
3	Al ribbon failure, interfacial failure, mixed failure	4, 5

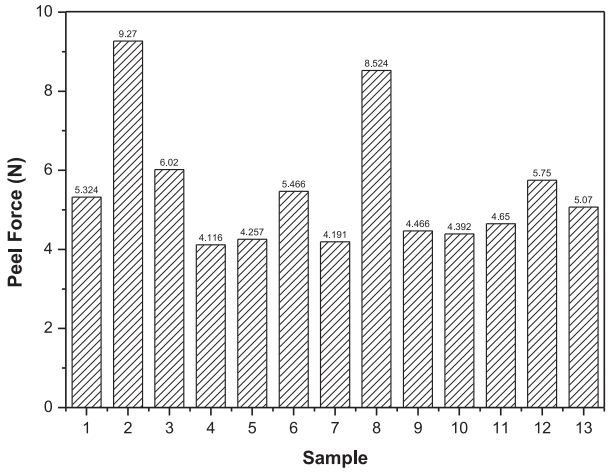

Fig. 10. Variation of peel force toward ultrasonic Al bonds.

load signify the bondability and the ductility or elongation of the Al ribbon [43], [44]. According to Zhao and Pelton [45], the load-distance profile could be divided into three failure modes namely interfacial failure, mixed failure, and paper failure. Zhao and Pelton [45] study has the similarity with the current analysis because paper, which has been used as sample in their study, had a rectangular shape and one of its ends was adhered to the substrate while the other end was not connected to any surface. They also reported that the distribution of the applied load during peel test is like that of metal with the critical stress being located at the interface of paper and substrate. Therefore, for the current study, the identification of failure modes of paper can be applied on the Al ribbon due to the similarity in terms of rectangular shape and the distribution of applied load during the peel test.

For the current analysis, it is noted that the Al ribbon, interfacial failure, and mixed failure occurred in the load-distance profiles with two and three segments as noted in Fig. 9(b) and (c), respectively, whereas Al ribbon failure occurred on the load-distance profile of Fig. 9(a). Table IV exhibits the list of load-distance profiles or samples with their respective segments and type of failure mode. Therefore, samples with one segment have the least failure mode of Al ribbon failure as compared to that of samples with two and three segments that have all three failure modes of Al ribbon, interfacial, and mixed failures.

The number of segments or failures modes also indicates the quality of the Al bond. This is because the type and number of failure modes represent the distribution and strength of the bonds. The samples with one segment of load-distance profiles

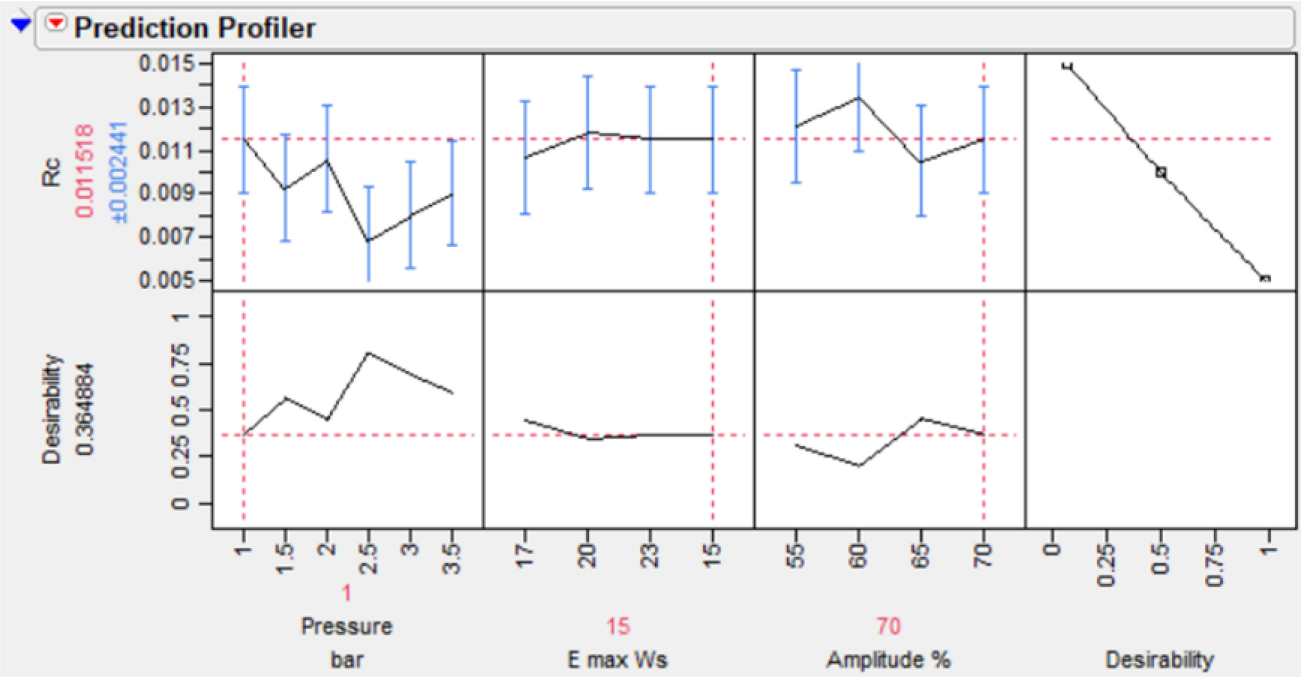

(a)

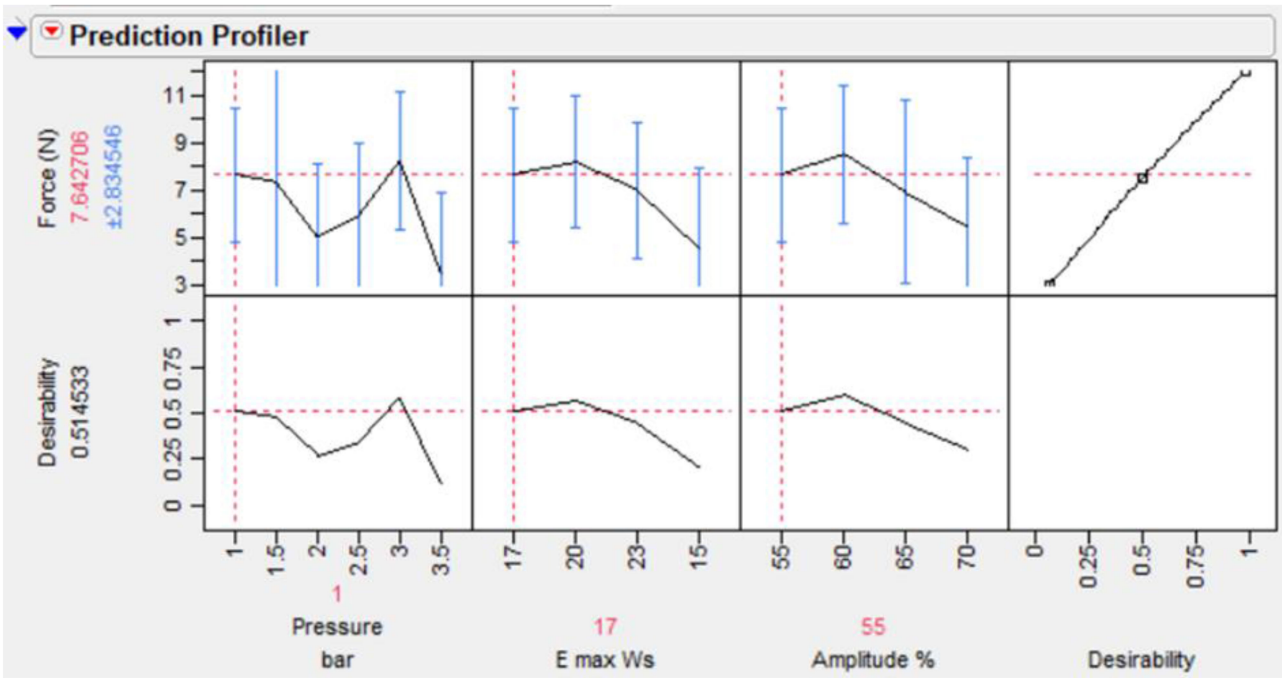

(b)

Fig. 11. Prediction profiler to determine the sensitivity of ultrasonic bonding parameter toward (a) *Rc* and (b) peel strength.

have higher peel force or strength as shown in Fig. 9(a). Furthermore, the failure mode of Al ribbon failure for the one segment load-distance profile signifies the higher distribution of adhesion of Al bond, where the weakest point is located at Al ribbon rather than the bond itself. On the other hand, samples with two and three segments of load-distance profiles indicate the weak adhesion at the bond area due to the occurrence of three different types of failure mode. Interfacial failure, particularly, indicates that samples with two and three segments of load-distance profiles have a weak bond. By referring to Fig. 9(b), it is noted that interfacial failure has load fluctuation with the least average slope as compared to that of mixed failure and Al ribbon failure. This shows that interfacial failure has an almost constant load with the least variation as compared to the other two failures. According to Chen and Zhang [46], the ultrasonic Al bonding can be divided into three periods, namely, the initial period, second period, and third period. Different bonding mechanisms are involved for each period with the growth rate of the contact

surface increases quickly in the initial period, decreases in the second period, and almost no changes in the third period. Takahashi *et al.* [33] also reported similar findings as Chen and Zhang [46] and reported that the growth rate of the contact surface is inversely related with the microweld or contact area that have been created. Thus, for the current study, the sample with one segment of the load-distance profile has the bond mostly covered with microweld or has reached the third period of ultrasonic bonding, whereas the sample with two or three segments of load-distance profiles might have least microweld or has reached the initial and second period of ultrasonic bonding.

Fig. 10 illustrates the variation of peel strength for each sample of ultrasonic bonds. In Fig. 10, the optimum peel strength of ultrasonic Al bond is identified based on the highest average peel force value [18]. It is noted that sample 2 has the highest peel force value of 9.27 N. This indicates that sample 2 with a parameter window of 3 bar of bonding pressure, 20 Ws of bonding energy, and 7.7 μm of bonding amplitude has the highest peel strength or bondability. As compared to that of Fig. 10, sample 2 has the fourth lowest R_c, while samples 12 and 13 have the lowest R_c. Therefore, to get higher peel strength and at the same time a quite lower R_c ultrasonic Al bond, sample 2 is the best-optimized bonding parameter window that can be applied.

D. Prediction Profiles

Fig. 11 shows the prediction profiles obtained from JMP software to determine the sensitivity of the ultrasonic bonding parameter toward R_c and peel strength. In Fig. 11(a), it is shown that the linear graph of top right corner of desirability box has a negative slope, whereas in Fig. 11(b), it has a positive slope. These indicate that the bonding parameter of bonding pressure, bonding energy, and bonding amplitude can be optimized by decreasing the R_c value and increasing the peel strength value. It is noted that bonding pressure is the highest sensitive parameter that can vary the R_c and peel strength significantly, followed by bonding amplitude and bonding energy. The sensitivity is identified through the number of slope changes of graphs in the bottom boxes, where bonding pressure has the most slope changes compared to that of bonding energy and bonding amplitude. In terms of manufacturability, the tolerance or sensitivity of the least bonding parameter of bonding energy can be relaxed or widened up to reduce the manufacturing cost. It is known that the manufacturing cost is proportional to the tolerance or sensitivity of the input parameter [47]. According to Jeang [48], the reduction of input parameter tolerance or sensitivity always leads to additional manufacturing cost due to the difficulty of the production machines to manufacture such product. Hence, the bonding pressure is the most sensitive bonding parameter with small tolerance, and bonding energy is the least sensitive bonding parameter with tolerance that could be relaxed to reduce the manufacturing cost of CIGS TFPV solar panel.

IV. Conclusion

Individual and combination of ultrasonic bonding parameter have shown to have a significant effect on the quality of Al bonds on Mo back contact layer of CIGS TFPV solar panel. It was noted that the application of higher bonding amplitude of 11.2 μm has created nonuniform ultrasonic Al bonds and a wavy shape of Al ribbon between each Al bond due to the excessive strain hardened and lack of elasticity of Al bond and ribbon. However, the application of higher bonding pressure of 4 bar has left only the footprint of the Al ribbon on the Mo layer and increased the potential of breaking the glass substrate, especially at the periphery or edge location. Application of higher bonding energy of 25 Ws has created an ultrasonic Al bond with inconsistent bond, shape (wavy and straight), and length of Al ribbon onto the Mo layer due to the combined effect of excessive ultrasonic softening and work hardening. The cumulative contact area between the Al bonds and ribbon has contributed toward decreasing the R_c that eventually increases the efficiency of CIGS TFPV solar panel, with samples 12 and 13 having the lowest R_c of 2.295 mΩcm^2. Samples with one segment of the load-distance profile have the least failure mode of Al ribbon failure as compared to that of samples with two and three segments that have all three failure modes of Al ribbon, interfacial, and mixed failures. Also, the sample with one segment of the load-distance profile has the bond mostly covered with microweld or has reached the third period of ultrasonic bonding, whereas sample with two or three segments of load-distance profiles might have least microweld or has reached the initial and second period of ultrasonic bonding. To get higher peel strength and lower R_c of ultrasonic Al bond, sample 2 is the best-optimized bonding parameter window that can be applied. Bonding pressure is the most sensitive bonding parameter with tight tolerance and bonding energy is the least sensitive bonding parameter with tolerance that could be relaxed to reduce the manufacturing cost of CIGS TFPV solar panel.

References

[1] V. Bermudez, "Economical and operational issues for CIGS in the future PV panorama," *Sol. Energy*, vol. 146, pp. 85–93, 2017.
[2] M. Powalla and B. Dimmler, "CIGS solar cells on the way to mass production: Process statistics of a 30 cm×30 cm module line," *Sol. Energy Mater. Sol. Cells*, vol. 67, no. 1–4, pp. 337–344, 2001.
[3] E. Schneller, N. G. Dhere, J. Shimada, and A. Kar, "Study of the laser scribing of molybdenum thin films fabricated using different deposition techniques," *Laser Mater. Process. Sol. Energy Devices II*, vol. 8826, 2013, Art. no. 88260C.
[4] F. Yan, D. J. Metacarpa, R. Sundaramoorthy, D. Fobare, and P. Haldar, "Evaluation of CIGS cell interconnection methods," in *Proc. IEEE 39th Photovolt. Specialists Conf.*, Jun. 2013, pp. 2064–2067.
[5] T. Xu, O. Valentin and C. Luechinger, "Reliable metallic tape connection on CIGS solar cells by ultrasonic bonding," *Thin Film Solar Technol. II*, vol. 7771, Aug. 2010, Art. no. 77710R.
[6] U. Eitner, T. Geipel, S. N. Holtschke, and M. Tranitz, "Characterization of electrically conductive adhesives," *Energy Procedia*, vol. 27, pp. 676–679, 2012.
[7] P. O. Westin, U. Zimmermann, M. Ruth, and M. Edoff, "Next generation interconnective laser patterning of CIGS thin film modules," *Sol. Energy Mater. Sol. Cells*, vol. 95, no. 4, pp. 1062–1068, 2011.
[8] E. J. Schneller *et al.*, "Manufacturing metrology for c-Si module reliability and durability Part III : Module manufacturing," *Renew. Sustain. Energy Rev.*, vol. 59, pp. 992–1016, 2016.
[9] D. Ren *et al.*, "Solar energy materials & solar cells glass transition temperature as an in situ cure index of electrically conductive adhesives in solar photovoltaic module interconnect assemblies," *Sol. Energy Mater. Sol. Cells*, vol. 107, pp. 403–406, 2012.
[10] G. Khatibi, B. Weiss, J. Bernardi, and S. Schwarz, "Microstructural investigation of interfacial features in Al wire bonds," *J. Electron. Mater.*, vol. 41, no. 12, pp. 3436–3446, 2012.

[11] S. Komarov, Y. Ishiwata, and I. Mikhailov, "Industrial application of ultrasonic vibrations to improve the structure of Al-Si hypereutectic alloys: Potential and limitations," *Metall. Mater. Trans. A Phys. Metall. Mater. Sci.*, vol. 46, no. 7, pp. 2876–2883, 2015.
[12] S. Mostafavi, D. F. Hesser, and B. Markert, "Effect of process parameters on the interface temperature in ultrasonic aluminum wire bonding," *J. Manuf. Process.*, vol. 36, pp. 104–114, Apr. 2018.
[13] A. Shah *et al.*, "Ultrasonic friction power during Al wire wedge-wedge bonding," *J. Appl. Phys.*, vol. 106, no. 1, Jul. 2009, Art. no. 013503.
[14] M. Li, H. Ji, C. Wang, H. S. Bang, and H. S. Bang, "Interdiffusion of Al-Ni system enhanced by ultrasonic vibration at ambient temperature," *Ultrasonics*, vol. 45, no. 1–4, pp. 61–65, 2006.
[15] R. Dohle, M. Petzold, R. Klengel, H. Schulze, and F. Rudolf, "Room temperature wedge–wedge ultrasonic bonding using aluminum coated copper wire," *Microelectron. Reliab.*, vol. 51, no. 1, pp. 97–106, Jan. 2011.
[16] P. Reinhard *et al.*, "Review of progress toward 20% efficiency flexible CIGS solar cells and manufacturing issues of solar modules," *IEEE J. Photovolt.*, vol. 3, no. 1, pp. 572–580, 2013.
[17] F. Kessler and D. Rudmann, "Technological aspects of flexible CIGS solar cells and modules," *Sol. Energy*, vol. 77, no. 6, pp. 685–695, 2004.
[18] A. Schneider, R. Harney, S. Aulehla, E. Lemp, and S. Koch, "Progress in interconnection of busbar-less solar cells by means of conductive gluing," *Energy Procedia*, vol. 38, pp. 387–394, 2013.
[19] M. Oertel *et al.*, "Measurement of the zinc oxide-molybdenum specific contact resistance for applications in Cu(In,Ga)Se_2-technology," *Thin Solid Films*, vol. 519, no. 21, pp. 7545–7548, 2011.
[20] M. Heimann *et al.*, "Ultrasonic bonding of aluminum ribbons to interconnect high-efficiency crystalline-silicon solar cells," *Energy Procedia*, vol. 27, pp. 670–675, Apr. 2012.
[21] D. C. Jordan, T. J. Silverman, B. Sekulic, and S. R. Kurtz, "PV degradation curves: Non-linearities and failure modes," *Prog. Photovolt. Res. Appl.*, vol. 25, no. 7, pp. 583–591, Jul. 2017.
[22] J. Pan, R. M. Pafchek, F. F. Judd, and J. B. Baxter, "Effect of chromium–gold and titanium–titanium nitride platinum–gold metallization on wire/ribbon bondability," *IEEE Trans. Adv. Packag.*, vol. 29, no. 4, pp. 707–713, Nov. 2006.
[23] S. Corthals, T. Witvrouwen, P. Jacobs, and B. Sels, "Development of dry reforming catalysts at elevated pressure: D-optimal vs. full factorial design," *Catal. Today*, vol. 159, no. 1, pp. 12–24, 2011.
[24] S. Guo, G. Gregory, A. M. Gabor, W. V. Schoenfeld, and K. O. Davis, "Detailed investigation of TLM contact resistance measurements on crystalline silicon solar cells," *Sol. Energy*, vol. 151, pp. 163–172, 2017.
[25] M. Heimann *et al.*, "Ultrasonic bonding of aluminum ribbons to interconnect high-efficiency crystalline-silicon solar cells," *Energy Procedia*, vol. 27, pp. 670–675, Apr. 2012.
[26] C. D. Breach and F. W. Wulff, "A brief review of selected aspects of the materials science of ball bonding," *Microelectron. Reliab.*, vol. 50, no. 1, pp. 1–20, Jan. 2010.
[27] J. E. Krzanowski and N. Murdeshwar, "Deformation and bonding processes in aluminum ultrasonic wire wedge bonding," *J. Electron. Mater.*, vol. 19, no. 9, pp. 919–928, 1990.
[28] J. van Deelen and C. Frijters, "CIGS cells with metallized front contact: Longer cells and higher efficiency," *Sol. Energy*, vol. 143, pp. 93–99, 2017.
[29] Y. Ding, J.-K. Kim, and P. Tong, "Numerical analysis of ultrasonic wire bonding: Effects of bonding parameters on contact pressure and frictional energy," *Mech. Mater.*, vol. 38, no. 1–2, pp. 11–24, Jan. 2006.
[30] M. Theelen and F. Daume, "Stability of Cu(In,Ga)Se_2 solar cells: A literature review," *Sol. Energy*, vol. 133, pp. 586–627, 2016.
[31] A. Shah *et al.*, "Ultrasonic friction power during thermosonic Au and Cu ball bonding," *J. Phys. D. Appl. Phys.*, vol. 43, no. 32, pp. 325301, Aug. 2010.
[32] Y. Zhou, X. Li, and N. J. N. J. Noolu, "A footprint study of bond initiation in gold wire crescent bonding," *IEEE Trans. Compon. Packag. Technol.*, vol. 28, no. 4, pp. 810–816, Dec. 2005.
[33] Y. Takahashi, K. Takashima, K. Misawa, and Y. Takaoka, "In-situ observation of adhesion behavior during ultrasonic Al ribbon bonding," *Appl. Sci.*, vol. 9, no. 9, pp. 34–39, 2019.
[34] H. Chai and B. R. Lawn, "A universal relation for edge chipping from sharp contacts in brittle materials: A simple means of toughness evaluation," *Acta Mater.*, vol. 55, no. 7, pp. 2555–2561, 2007.
[35] H. Chai, "On the mechanics of edge chipping from spherical indentation," *Int. J. Fract.*, vol. 169, no. 1, pp. 85–95, 2011.
[36] T. M. Gross, "Deformation and cracking behavior of glasses indented with diamond tips of various sharpness," *J. Non. Cryst. Solids*, vol. 358, no. 24, pp. 3445–3452, 2012.
[37] G. S. Kelly, M. S. Just, S. G. Advani, and J. W. Gillespie, "Energy and bond strength development during ultrasonic consolidation," *J. Mater. Process. Technol.*, vol. 214, no. 8, pp. 1665–1672, 2014.
[38] M. N. Zulkifli, F. Harun, and A. Jalar, "Effect of surface roughness and hardness of leadframe on the bondability of gold wedge bonds," *Microelectron. Int.,* vol. 36, no. 2, pp. 62–67, 2019.
[39] B. Langenecker, "Effects of ultrasound on deformation characteristics of metals," *IEEE Trans. Sonics Ultrason.*, vol. 13, no. 1, pp. 1–8, Mar. 1966.
[40] M. N. Zulkifli, S. Abdullah, N. K. Othman, and A. Jalar, "Some thoughts on bondability and strength of gold wire bonding," *Gold Bull*, vol. 45, no. 3, pp. 115–125, Sep. 2012.
[41] E. Markauskas, P. Gečys, A. Žemaitis, M. Gedvilas, and G. Račiukaitis, "Validation of monolithic interconnection conductivity in laser scribed CIGS thin-film solar cells," *Sol. Energy*, vol. 120, pp. 35–43, 2015.
[42] K. L. Chopra, P. D. Paulson, and V. Dutta, "Thin-film solar cells: An overview," *Prog. Photovolt. Res. Appl.*, vol. 12, no. 23, pp. 69–92, Mar. 2004.
[43] M. Barquins and M. Ciccotti, "On the kinetics of peeling of an adhesive tape under a constant imposed load," *Int. J. Adhes. Adhes.*, vol. 17, no. 1, pp. 65–68, 1997.
[44] N. Saiki, K. Inaba, K. Kishimoto, H. Seno, and K. Ebe, "Study on peeling behavior in pick-up process of IC chip with adhesive tapes," *J. Solid Mech. Mater. Eng.*, vol. 4, no. 7, pp. 1051–1060, 2010.
[45] B. Zhao and R. Pelton, "Peel adhesion to paper—Interpreting peel curves," *J. Adhes. Sci. Technol.*, vol. 17, no. 6, pp. 815–830, 2003.
[46] K. Chen and Y. Zhang, "Mechanical analysis of ultrasonic welding considering knurl pattern of sonotrode tip," *Mater. Des.*, vol. 87, pp. 393–404, 2015.
[47] M. N. Zulkifli, Z. A. Z. Jamal, and G. A. Quadir, "Temperature cycling analysis for ball grid array package using finite element analysis," *Microelectron. Int*, vol. 28, no. 1, pp. 17–28, 2011.
[48] A. Jeang, "Combined parameter and tolerance design optimization with quality and cost," *Int. J. Prod. Res.*, vol. 39, no. 5, pp. 923–952, 2001.